International Journal of Nanomedicine

Dovepress
open access to scientific and medical research

Open Access Full Text Article

ORIGINAL RESEARCH

IL-12-Overexpressed Nanoparticles Suppress the Proliferation of Melanoma Through Inducing ICD and Activating DC, $CD8^+$ T, and $CD4^+$ T Cells

Huan-Huan Shen[1,2,*], Jie-Fei Peng[1,3,*], Ran-Ran Wang[4,*], Ping-Yu Wang[1,5], Jia-Xiang Zhang[1], Hong-Fang Sun[1], Yan Liang[1], Yan-Mei Li[6], Jiang-Nan Xue[7], You-Jie Li[1], Guang-Bin Sun[1,*], Shu-Yang Xie[1,2,*]

[1]Department of Biochemistry and Molecular Biology, Binzhou Medical University, YanTai, Shandong, 264003, People's Republic of China; [2]Shandong Laboratory of Advanced Materials and Green Manufacturing, Yantai, Shandong, 264000, People's Republic of China; [3]Department of Clinical Laboratory, the Affiliated Taian City Central Hospital of Qingdao University, Taian, 271000, People's Republic of China; [4]Institute of Rehabilitation Medicine, School of Rehabilitation Medicine, Binzhou Medical University, Yantai, Shandong, 264003, People's Republic of China; [5]Department of Epidemiology, Binzhou Medical University, YanTai, ShanDong, 264003, People's Republic of China; [6]Department of Immune Rheumatism, Yantaishan Hospital, Yantai, Shandong, 264000, People's Republic of China; [7]Department of Immunology, Binzhou Medical University, Yantai, Shandong, 264003, People's Republic of China

*These authors contributed equally to this work

Correspondence: Shu-Yang Xie; Guang-Bin Sun, Department of Biochemistry and Molecular Biology, Binzhou Medical University, YanTai, Shandong, 264003, People's Republic of China, Tel +86 535 6913010; +86 535 6913335, Fax +86 535 6913163, Email xieshuyang@bzmc.edu.cn; bingo@bzmc.edu.cn

Purpose: The drug resistance and low response rates of immunotherapy limit its application. This study aimed to construct a new nanoparticle ($CaCO_3$-polydopamine-polyethylenimine, CPP) to effectively deliver interleukin-12 (IL-12) and suppress cancer progress through immunotherapy.

Methods: The size distribution of CPP and its zeta potential were measured using a Malvern Zetasizer Nano-ZS90. The morphology and electrophoresis tentative delay of CPP were analyzed using a JEM-1400 transmission electron microscope and an ultraviolet spectrophotometer, respectively. Cell proliferation was analyzed by MTT assay. Proteins were analyzed by Western blot. IL-12 and HMGB1 levels were estimated by ELISA kits. Live/dead staining assay was performed using a Calcein-AM/PI kit. ATP production was detected using an ATP assay kit. The xenografts in vivo were estimated in C57BL/6 mice. The levels of $CD80^+$/$CD86^+$, $CD3^+$/$CD4^+$ and $CD3^+$/$CD8^+$ were analyzed by flow cytometry.

Results: CPP could effectively express EGFP or IL-12 and increase ROS levels. Laser treatment promoted CPP-IL-12 induced the number of dead or apoptotic cell. CPP-IL-12 and laser could further enhance CALR levels and extracellular HMGB1 levels and decrease intracellular HMGB1 and ATP levels, indicating that it may induce immunogenic cell death (ICD). The tumors and weights of xenografts in CPP-IL-12 or laser-treated mice were significantly reduced than in controls. The IL-12 expression, the $CD80^+$/$CD86^+$ expression of DC from lymph glands, and the number of $CD3^+$/$CD8^+$T or $CD3^+$/$CD4^+$T cells from the spleen increased in CPP-IL-12-treated or laser-treated xenografts compared with controls. The levels of granzyme B, IFN-γ, and TNF-α in the serum of CPP-IL-12-treated mice increased. Interestingly, CPP-IL-12 treatment in local xenografts in the back of mice could effectively inhibit the growth of the distant untreated tumor.

Conclusion: The novel CPP-IL-12 could overexpress IL-12 in melanoma cells and achieve immunotherapy to melanoma through inducing ICD, activating $CD4^+$ T cell, and enhancing the function of tumor-reactive $CD8^+$ T cells.

Keywords: cancer immunotherapy, $CaCO_3$ nanoparticle, interleukin-12, immunogenic cell death, tumor therapy

Introduction

At present, cancer therapy methods include surgery, radiotherapy, chemotherapy, gene therapy, photothermal therapy (PTT), and immunotherapy. Compared with their organic and polymeric counterparts, inorganic nanoparticles have unique features, and they are widely used for therapy and diagnosis.[1] Therefore, great inorganic nanoparticles with low cytotoxicity and high biocompatibility to deliver small molecules are essential in cancer therapy. Among different

Received: 28 September 2023
Accepted: 5 March 2024
Published: 18 March 2024

inorganic biominerals, $CaCO_3$ nanoparticles have been used for the controlled and sustained delivery of photosensitizers,[2] chemical drugs,[3] and nucleic acids[4] because of their low biological toxicity, high ideal biocompatibility, and photoimmunotherapy. $CaCO_3$ is stable at physiological and neutral pH, but it dissociated at acidic conditions.[5] Based on previous reports, $CaCO_3$ have longer biodegradation times. When $CaCO_3$ is used as a gene vector to transfect pDNA into cells, polyethylenimine (PEI) is an appropriate reagent for the surface modification of nanoparticles due to its high DNA complexation ability and strong proton sponge effect, which endows PEI/DNA complexes with the capacity to disrupt endo-lysosomes.[6,7]. Photothermal therapy is a promising technique, in which heat is generated from near-infrared light by using a highly efficient photothermal agent to ablate cancer cell, and it presents many advantages such as high efficacy, low systemic toxicity, noninvasiveness, and no injury to normal tissues.[8] PTT could increase the permeability of the cell membrane to enhance cellular uptake and gene transfection efficiency.[9] PTT could also induce immunogenic cell death (ICD). Thus, nanoparticles could achieve enhanced antitumor effects when combined with immune boosting components, such as immune adjuvants, adoptive T/NK cells, and immune checkpoint inhibitors.[10,11] Among the various photothermal agents, polydopamine (PDA) is considered as more promising PTT agent owing to the advantages of excellent biocompatibility, good biodegradability and high photothermal conversion efficiency.[12–14]

Cytokines are the major components in regulating immune responses, thus, they show potential application in cancer immunotherapy.[15] IL-12 is a cytokine primarily produced by activated monocytes, macrophages, dendritic cells and other antigen-presenting cells (APCs).[16] It is involved in type 1 helper T cell differentiation, natural killer cells and cytotoxic T lymphocyte proliferation.[17,18] IL-12 plays a key role in antitumor immunity, which may be an effective adjuvant for chimeric antigen receptor T-Cell immunotherapy (CAR-T immunotherapy) for cancer.[19] However, injection of IL-12 gene at tumor sites may be a better strategy than injection of IL-12 protein to achieve an antitumor effect because of the short half-life of IL-12 protein.[20] Therefore, PTT and immunotherapy were applied in the present study, $CaCO_3$-polydopamine (PDA)-PEI nanoparticles were constructed to deliver IL-12-overexpressed plasmids (CPP-IL-12) and investigate the roles of CPP-IL-12 in cancer therapy. As for the designed nanoparticles, $CaCO_3$ has good accessibility, biocompatibility, and pH sensitivity, which can generate carbon dioxide and Ca^{2+} in tumor microenvironment.[21] PDA is suitable for PTT, and PEI is an appropriate reagent to stabilize DNA from degradation and improve gene release.[22] IL-12 expression from plasmids is important for tumor therapy. The production of Ca^{2+} in tumor microenvironment is crucial for ICD by upregulating reactive oxygen species (ROS) levels.[23] The results of the present study showed that CPP can effectively deliver IL-12 in cancer cells and suppress cell proliferation through PTT and immunotherapy.

Materials and Methods

Preparation of Nanomaterials

The designed multifunctional calcium-based nanoparticles were prepared as follows. First, 150 mg $CaCl_2$ and 10 mg PDA were completely dissolved in 100 mL absolute ethanol, and then 85 mg of PEI was added and dissolved. Five grams of ammonium bicarbonate was added at 40°C, and the mixture was stored for 24 h. The supernatant was discarded, and the precipitate was washed with absolute ethanol three times and collected to obtain CPP. The size distribution of CPP and its zeta potential were measured using a Malvern Zetasizer Nano-ZS90 (Malvern, UK). The morphology of CPP was analyzed using a JEM-1400 transmission electron microscope (JEOL, Japan). The concentration-dependent temperature curves of CPP were detected using an 808 nm laser from Daheng Optoelectronics (China). The photothermal heating curves of the material were continuously monitored for three cycles.

Agarose Electrophoretic Analysis

CPP and pEGFP-N1 (EGFP, Clontech, USA) were mixed at different weight ratios of 10:1, 20:1, 30:1, 40:1, and 50:1, and then incubated in sterile water at room temperature for 30 min. The electrophoresis gels were analyzed using a gel imager (Tanon 2500, Shanghai).

Infrared Spectroscopic Analysis

The materials were centrifugally dried to prepare a powder, and infrared spectroscopy was performed using KBr tableting with an infrared spectrometer (Nicolet iS10, Thermo Scientific, Shanghai, China).

Cell Culture

Mouse embryonic fibroblast cells (NIH3T3) and mouse melanoma cells (B16-F10) were purchased from Shanghai Institute of Cell Biology (Shanghai, China). These cell lines were cultured in Dulbecco's Modified Eagle Medium (Thermo Fisher Scientific, MA, USA) supplemented with 10% fetal bovine serum (FBS), 100 units/mL penicillin and 100μg/mL streptomycin in a humidified atmosphere containing 5% CO_2 at 37°C.

3-(4,5-Dimethylthiazol-2-Yl)-2,5-Diphenyltetrazolium Bromide (MTT) Assay

Cells proliferation was analyzed by MTT assay following the previous reports.[24,25] In brief, cells (1×10^4) were cultured in each well of a 96-well flat bottom microtiter plates. Four hours before the end of incubation, each well was added with 10 μL MTT (Sigma, St Louis, MO, USA, 5 mg/mL). After the supernatant was removed, 100 μL DMSO (Sigma) was added and the optical density (OD) was estimated at 570 nm using an ELISA reader (Multiskan FC, Thermo Fisher Scientific, MA, USA).

ROS Detection in vitro

The ROS generation in CPP and control groups was analyzed by using an ROS assay kit (CA1410, Solarbio Science & Technology Co., Ltd., Beijing, China) in accordance with the manufacturer's instructions. The 2′,7′-Dichlorodihydrofluorescein Diacetate (DCFH-DA) probe solution was added to react for 0.5 h. ROS generation was analyzed using a fluorescence spectrophotometer (Hitachi F-2700, Japan).

Western Blot

Western blot analysis was performed as in previous reports.[24,25] Membranes were incubated with rabbit anti-mouse IL-12 (1:500, LSBio, Seattle WA, USA) and β-actin (1:3000, Bioworld Technology, Ltd., Nanjing, China) in tris buffered saline with Tween-20 (TBST) at 4°C overnight. HRP-labeled goat anti-rabbit IgG (1:6000, Zhong Shan-Golden Bridge Technology Co., Ltd., Beijing, China) was added for 1 h. Immunoblotting was incubated with enhanced chemiluminescence (ECL) (Boster Immunoleader, Wuhan, China).

ELISA

IL-12 and HMGB1 levels were estimated using ELISA kits (CSB-E04600m and CSB-E08225M, CUSABIO, Wuhan, China) in accordance with the manufacturer′s instructions. In brief, 100 μL of the standard and sample was added per well and incubated for 2 h at 37°C. After the liquid of each well was removed, 100 μL biotin antibody was added, and the mixture was incubated for 1 h at 37°C. Next, 100 μL HRP-Avidin was added for 1 h at 37°C. TMB substrate was added, and data were analyzed at 450 nm using an ELISA reader (Multiskan FC, Thermo Fisher Scientific).

Live/Dead Staining

Live/dead staining assay was performed using a Calcein-AM/PI kit (CA1630, Solarbio, Beijing, China). B16-F10 cells were collected, and the supernatant was removed. Cell suspensions were prepared with a density of 1×10^5 cells/mL. Staining working solution (100 μL) was added to 200 μL cell suspensions, and the mixture was incubated at 37°C for 15 min. Then, the cells were observed under a confocal microscope (LEICA TCS SPE, Leica, Dresden, Germany).

Apoptosis Assays

Apoptotic B16-F10 cells were analyzed using an Annexin V-FITC/PI kit (KeyGEN Biotech. Co. Ltd., Nanjing, China) following the manufacturer′s instruction. A total of 1×10^5 cells were analyzed using flow cytometry as previously reported.[24]

Intracellular Ca^{2+} Level Analysis

Fluo-3AM fluorescent dye was used to detect intracellular Ca^{2+} levels. In brief, B16-F10 cells were centrifuged and washed twice with Hank's without calcium and magnesium, then 0.5–5 μM Fluo-3AM solution was added. The cells were incubated at 37°C in the dark for 30–40 min. The cells were observed under a fluorescence microscope. Fluo-3 was green fluorescence. Next, the cells were gently purged with Hank's without calcium and magnesium to fully wash the residual fluorescent dye, and the fluorescence was measured by flow cytometry.

Immunofluorescence

Immunofluorescence analysis of calreticulin levels was performed as described in a previous study.[25] Cells were prepared and incubated with rabbit anti-calreticulin antibody (1:200, Abcam, San Francisco, CA, USA) overnight at 4 °C, and then with Alexa Fluor 488 donkey anti-rabbit IgG (H+L, Molecular Probes, Eugene, OR, USA) at 37 °C for 1 h. The results were observed under a confocal microscope (LEICA TCS SPE, Leica, Dresden, Germany).

ATP Content

The ATP levels in CPP-IL-12-treated B16-F10 cells was detected using ATP production was detected by using ATP assay kit in accordance with the manufacturer's instructions (BC0305, Solarbio, Beijing, China).

Xenografts in C57BL/6 Mice

C57BL/6 mice were purchased from Jinan Aonuo Bio (Shandong, China). All mice aged 6–8 weeks were housed in a specific pathogen-free Animal Center of Binzhou Medical University (Yantai, China). Care and experiments for mice were performed according to Binzhou Medical University animal ethical guidelines for Laboratory Animal Care, and were approved by the Animal Ethics Committee of Binzhou Medical University (No. 2020-01-02, Yantai, China).

Melanoma cells (5×10^6) in 0.1 mL of PBS treated with CPP-IL-12 and controls were transplanted subcutaneously into the backs of C57BL/6 mice. One week later, the tumors grew about 1 cm^3, which were further treated with 100 μL of CPP-IL-12 (1 mg/mL) or CPP-NC (negative control plasmid) with or without laser treatment (1.5 weeks, 3 min) for 2 days. Tumor volume (mm^3) = $A \times B^2/2$, where A and B are the maximum and minimum tumor diameters, respectively. At day 15, the mice were euthanized, and the tumors were anatomized and weighed. The investigator had no bias and special tendency during animal experiments.

To investigate whether CPP-IL-12 treatment in local side xenografts can affect the growth of the distant untreated side, melanoma cells (5×10^6) in 0.1 mL of PBS were transplanted subcutaneously into one side in the back of C57BL/6 mouse. The local tumor was treated with 100 μL of CPP-IL-12 (1 mg/mL) and laser (1.5 weeks, 3 min) for 2 days. Three days later, the distant side was transplanted subcutaneously with melanoma cells without treatment of CPP-IL-12. The xenografts were then observed.

In detecting the toxicity of CPP in vivo, the CY5.5-labeled CPP was injected through the tail vein of C57BL/6 mice and analyzed using a small animal PET imager system (IVIS spectrum, PE, USA).

Hemolytic Test

Blood samples from C57BL/6 mice were collected, centrifuged at 800 g for 5 min, and washed five times with PBS. Fresh erythrocyte suspension (50 μL) was added to 1 mL CPP suspension at room temperature. At different incubation times, 200 μL of the erythrocyte suspension was centrifuged, collected, and placed in a 96-well plate to detect the absorbance value at 540 nm using a Multiskan FC-type microplate reader (Thermo Fisher Scientific.). A positive control (100% hemolyzed) was prepared by adding the red blood cell suspension with 1 mL water. A negative control was obtained by adding the erythrocyte suspension with 1 mL PBS.

Flow Cytometry Analysis

For DC from bone marrow, C57BL/6 mice (Jinan Aonuo Bio, Shandong, China) were euthanized and soaked in 75% alcohol for 30 min. The femurs of lower limbs were dissected and placed in PBS with 10% FBS. The holes were punched

at both ends of the femur using a 20 mL syringe needle, and bone marrow was flushed out using a 1 mL syringe. The washed bone marrow was resuspended, and 1×10^5 bone marrow cells were cultured in RPMI 1640 medium of 10% FBS with GM-CSF (10 ng/mL) and IL-4 (10 ng/mL, BioLegend, San Diego, CA, USA). The floating cells were removed after 24 h, and the medium was added again. Then, the DCs were treated with the supernatant of B16-F10 cells: complete medium (1:1). After 24 h, the DCs were freshly collected and stained with antibodies for 30 min at 4°C. Flow cytometry was performed to analyze the data (Accuri™ C6, BD, USA). The following monoclonal anti-mouse antibodies were used: anti-CD80-PE/Cy5.5 (BioLegend, USA) and anti-CD86-APC (BioLegend, USA).

For treatment of xenografts, the mice were euthanized and the lymph glands were isolated from groins, armpits, and necks. The lymph glands were sheared and filtered through 19 μm nylon mesh. The cells were stained with $CD80^+$/$CD86^+$ antibodies for 30 min at 4 °C and analyzed by flow cytometry. Similarly, the spleens of C57BL/6 mice were sheared and filtered through 19 μm nylon mesh. The cells were stained with $CD3^+$/$CD4^+$ and $CD3^+$/$CD8^+$ antibodies for 30 min at 4°C and analyzed by flow cytometry. The following monoclonal anti-mouse antibodies were used: anti-CD3-APC (Biolegend), anti-CD4-PE (Biolegend), and anti-CD8-FITC (Biolegend).

HE Staining and Immunohistochemistry

Tumor xenografts or organs of mice were dissected, fixed in 4% paraformaldehyde, automatically dehydrated, embedded in paraffin, sectioned, and stained with HE. Then, the sections were observed under a microscope (Leica DM6000b, Germany).

For immunohistochemistry, the sections of xenografts were deparaffinized and rehydrated in alcohol. The endogenous peroxidase activity in tissues was inactivated by 3% hydrogen peroxide for 15 min. Then, the sections were washed with PBS and incubated in 10% normal goat serum (BeiJingZhongShan Golden Bridge Technology Co, Ltd., Beijing) for 20 min. Next, the sections were incubated with rabbit anti-IL-12 primary antibodies (1:300, Bioworld Technology, Ltd.) at 4°C overnight. Next, these sections were combined with biotin-conjugated goat anti-rabbit IgG (1:200, dilution, Santa Cruz Biotechnology, Inc.). The slides were incubated with the avidin-biotin complex and developed in 3,3-diaminobenzidine solution (Santa Cruz Biotechnology, Inc.). Negative controls were stained with non-immune serum.

Statistics

SPSS 22.0 software is used to analyze statistical significance (IBM Corp., Armonk, NY, USA). Normally distributed data were shown as mean ± SD. Two groups and multiple groups were compared by Student's *t* test and ANOVA, respectively. Abnormally distributed data were presented as median (interquartile range), two groups and multiple groups were compared by Mann–Whitney *U*-test and Kruskal–Wallis *H*-test, respectively. $p< 0.05$ was considered as statistically significant difference.

Results

Synthesis and Characterization of Nanoparticles

Recently, the application of $CaCO_3$ nanoparticles has received considerable interest as a gene delivery system for cancer therapy because of their low cost, safety, pH sensitivity, and biocompatibility.[26] Polydopamine, as a mussel-inspired molecule, has been applied in cancer therapy because of its good biocompatibility, low tissue toxicity, outstanding drug-loading capacity, and degradability.[27] Here, a $CaCO_3$-PDA-PEI (CPP) nanoparticle was designed and synthesized to investigate its role in delivering IL-12 for the treatment of melanoma cells (Figure 1A). Its particle size was approximately 270 ± 10 nm, and the potential was approximately +25 mV (Figure 1B and C). CPP showed a monodisperse spherical nanostructure (Figure 1D).

The chemical composition of CPP was analyzed by Fourier transform infrared spectroscopy (Figure 1E). The strong absorption signals of PEI clearly shown in the spectrum were 2961 and 2930 cm^{-1}. The C-O stretching vibration peak was 1756 cm^{-1}, and the C-O antisymmetric stretching vibration was 1432 cm^{-1}. The CO_3^- deformation vibration peak was 876 cm^{-1}. The characteristic absorption peaks of $CaCO_3$ were as follows: 1756, 1432, 876, and 724 cm^{-1} (Figure 1E).

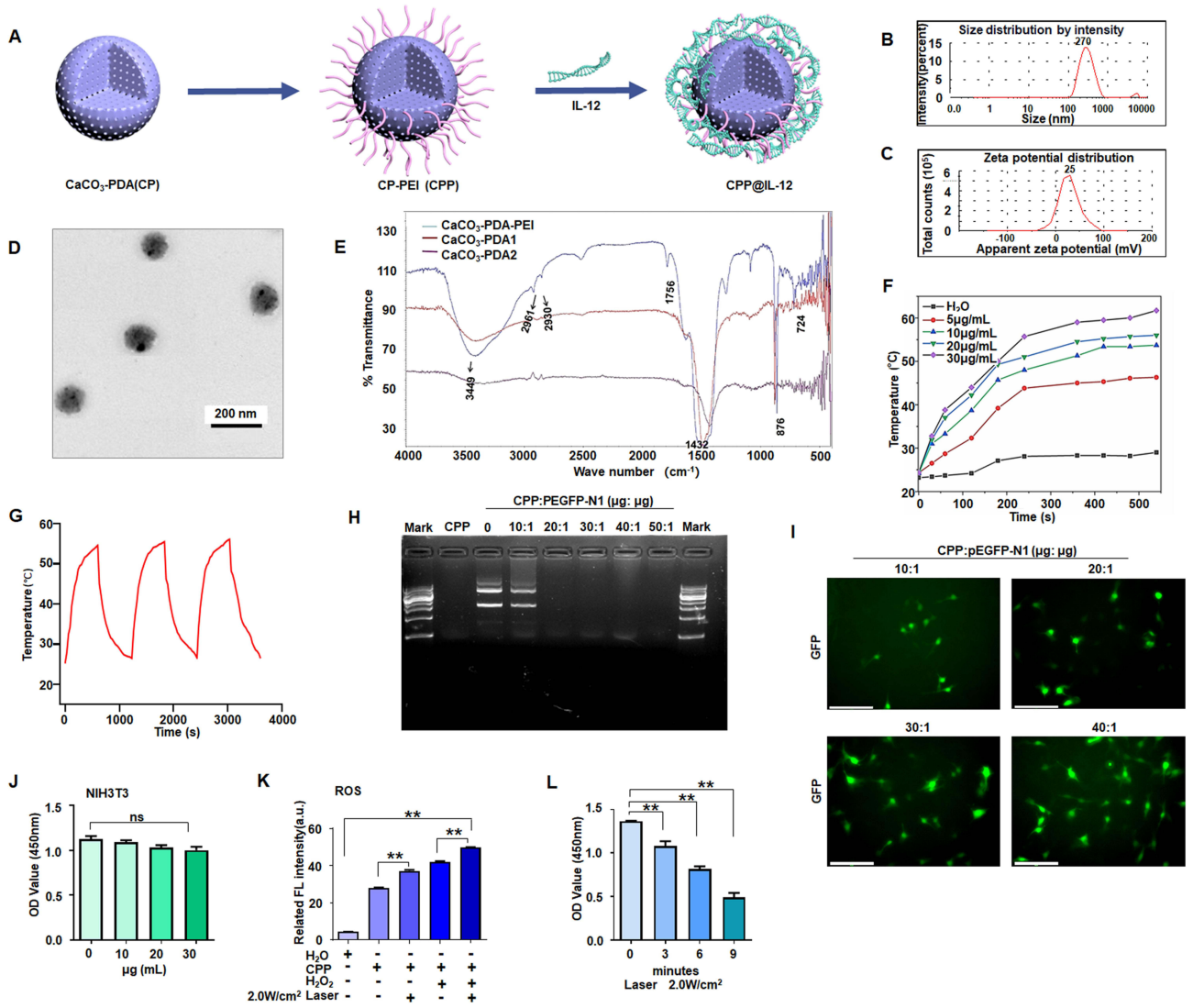

Figure 1 CPP inhibited cancer cell proliferation. (**A**) Schematic illustration of the synthesis of CPP-IL-12. (**B**) Size distribution of CPP. (**C**) The average zeta potentials of CPP. (**D**) Transmission Electron Microscope images of CPP. Scale bars=200 nm. (**E**) The chemical composition was analyzed by Fourier transform infrared spectroscopy. (**F**) Heating curves of different concentrations of CPP under 808 nm (2 W/cm^2) laser irradiation. (**G**) The photothermal conversion cycling test of CPP during three cycles of laser on/off. The data are presented as the mean ± SD of three independent experiments. (**H**) Electrophoretic analysis of pEGFP plasmid in the complexes of CPP under various N/P ratios. (**I**) B16F10 cells incubated with CPP@pEGFP complexes (N/P from 10:1 to 40:1); green colour, EGFP expression. Scale bars=125 μm. (**J**) Analyzing the cytotoxicity of CPP, ANOVA. (**K**) ROS detection. CPP treatment increased ROS levels, and 2.0 W/cm^2 of laser further increased ROS levels. $^{**}P<0.01$, ANOVA. (**L**) Cell proliferation analysis. B16-F10 cell proliferation was suppressed at 3 min to 9 min after laser treatment, $^{**}P<0.01$, ANOVA.

Then, the changes in the heating curve of CPP at different concentrations were analyzed under laser irradiation. The temperature of CPP gradually increased from 5 μg/mL to 30 μg/mL over time, reaching the maximum at 10 min. The changes were not significant after 10 min. After three consecutive heating cycles, the temperature of CPP (20 μg/mL) did not change significantly. These data demonstrated that the nanoparticles had good thermal stability (Figure 1F and G).

Laser's Promotion of the Effect of Nanoparticles

Nanoparticles serve as a carrier to deliver DNA/RNA for cancer therapy, and they have several advantages, such as photosensitive therapy by laser irradiation. The designed CPP nanoparticles with PEI can carry DNA/plasmids through electrostatic interaction. The gene condensation ability of CPP was analyzed by agarose gel electrophoresis. As shown in (Figure 1H), CPP can completely condense the pEGFP-N1 plasmid (EGFP expression vector) when the CPP/N1 ratio was above 20:1. EGFP was effectively expressed in B16-F10 cells when the cells were treated with CPP-EGFP

nanoparticles with the CPP/EGFP ratio above 20:1 (Figure 1I). Therefore, the CPP/EGFP ratio of 20:1 was selected for this study. NIH3T3 cells were treated with different concentrations (10─30 μg/mL) of CPP to test its cytotoxicity. Compared with the control, no evident cytotoxicity to NIH3T3 cells was found when the nanomaterial dose was increased (Figure 1J). Thus, 20 μg/mL CPP was selected as the transfecting concentration.

The overabundance of ROS in cancer cells remains a challenge in therapeutic intervention, and nanotechnology has been remarkably developed to alter redox status and improve conventional therapies.[28] $CaCO_3$ has good biocompatibility, and it can produce ROS after low-intensity ultrasound treatment.[29] Therefore, the ROS levels in the CPP-treated group were determined, and the results showed that the ROS levels in the CPP-treated group significantly increased compared with those in the negative control (H_2O), and 2.0 W/cm^2 laser treatment could further increase the ROS levels (Figure 1K). Laser treatment also increased ROS levels in the positive control H_2O_2-treated group (Figure 1K).

B16-F10 cells were treated with 20 μg/mL CPP-PEI and laser irradiation (808 nm, 2.0 W/cm^2) to investigate the role of CPP and radiation therapy via enhancing ROS production in regulating cell proliferation. The results demonstrated that B16-F10 cell proliferation was significantly suppressed at 3, 6, or 9 min after laser treatment, and the laser treatment time of 6 min was the best time for radiation therapy (Figure 1L).

Gene Delivery of IL-12 and Inducing B16-F10 Cell Apoptosis

IL-12 is responsible for enhancing cell-mediated immunity, and it has demonstrated remarkable antitumor effects against various malignancies in preclinical studies.[30] The IL-12 overexpression vector was constructed to study the delivery of IL-12 into B16-F10 cells and its effect on cancer cell apoptosis (Figure 2A), and CPP was designed to condense the IL-12 plasmid. The results demonstrated that the IL-12 levels were significantly higher in CPP-IL-12-treated B16-F10 cells than in the control group (Figure 2B). ELISA analysis showed higher IL-12 levels in the supernatant of CPP-IL-12-treated B16-F10 cells, and 2.0 W/cm^2 laser treatment further increased the IL-12 levels in the supernatant (Figure 2C). The live/dead staining assay results showed more dead cells in CPP-IL-12-treated B16-F10 cells than in the CPP-NC control. Laser treatment increased the number of dead cells (Figure 2D and E). CPP-IL-12 treatment induced B16-F10 cell apoptosis, and laser treatment can further increase the apoptotic number of B16-F10 cells (Figure 2F).

CPP-IL-12 Induced ICD

Cancer immunotherapies can eradicate tumor cells with slight damage to healthy cells and demonstrate potential clinical responses.[31] Some drugs can induce ICD, which directly kills cancer cells and induces antitumor immune responses against various tumors.[31] Previous studies reported that $CaCO_3$ has pH sensitivity and can generate Ca^{2+} in tumor microenvironment, which is crucial for ICD.[21] Meanwhile, ICD is accompanied by releasing numerous damage-associated molecular patterns (DAMPs), including surface-exposed calreticulin (CALR), ATP, and high-mobility group box 1 (HMGB1), which recruits and APCs to kill tumor cells.[32] As $CaCO_3$ nanoparticle can effectively deliver and express IL-12, whether the effect of $CaCO_3$ nanoparticle on tumor cells through ICD was investigated. First, the intracellular Ca^{2+} levels were detected using calcium ion fluorescence probe. The results demonstrated that the intracellular Ca^{2+} levels in the CPP-treated cells increased obviously compared with those of the control group (Figure S1), indicating that CPP can generate Ca^{2+} in tumor microenvironment. Next, the DAMPs levels were analyzed after $CaCO_3$ nanoparticle treatment. The results showed that CPP-IL-12 increased the CALR levels in B16-F10 cells, and laser treatment (2.0 W/cm^2) can further enhance CALR expression compared with control treatment (Figure 2G). In addition, the extracellular HMGB1 levels significantly increased and the intracellular HMGB1 levels decreased in CPP-IL-12-treated cultures compared with those in the control group (Figure 2H and I). Laser treatment (2.0 W/cm^2) further enhanced the HMGB1 levels in CPP-IL-12-treated cultures compared with control treatment (Figure 2I). The ATP levels in CPP-IL-12-treated B16-F10 cells decreased compared with those in the CPP-Con group, and laser treatment further reduced the ATP content in the CPP-IL-12-treated cultures (Figure 2J). These results showed that CPP-IL-12 can induce ICD in B16-F10 cells.

At present, the application of DC-based immunotherapy in cancer treatment is safe and feasible.[33] Emerging evidence supports that ICD-induced therapies are strictly associated with DC engagement.[33] The DCs from the bone marrow of C57BL/6 mice were treated with the supernatant of B16-F10 cells, and the results showed that CPP-IL-12 treatment (21.4%) and laser treatment (2.0 W/cm^2) further increased the $CD80^+/CD86^+$ expression (29.2%) of DC compared with control treatment (11.2% or 12.6%, Figure 2K), indicating that ICD induced by CPP-IL-12 is related to the activation of DC.

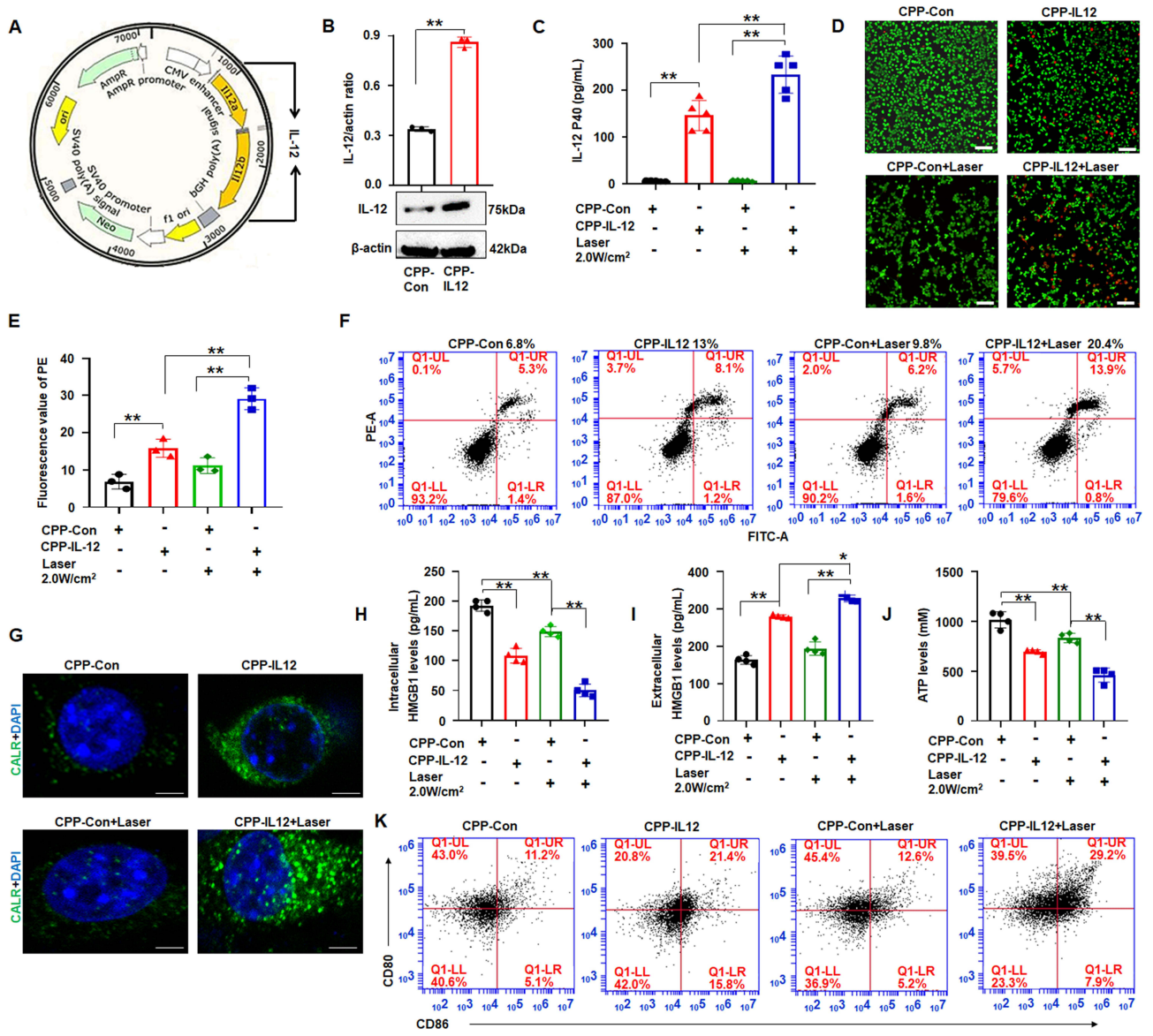

Figure 2 CPP transferred IL-12 into B16F10 cells and CPP-IL-12 induced immunogenic cell death. (**A**) The structure of IL-12 vector. (**B**) Western blot detection of IL-12 expression. $^{**}P < 0.01$, Student's *t*-test. (**C**) ELISA. CPP-IL-12 increased IL-12 levels in the supernatant of B16-F10 cells, and 2.0 W/cm^2 of laser further increased IL-12 levels. $^{**}P < 0.01$, ANOVA. (**D**) Live/dead staining assay. Scale bars=100 μm. (**E**) The number of dead cells. CPP-IL-12 increased and 2.0 W/cm^2 of laser further increased the number of dead cells. $^{**}P < 0.01$, ANOVA. (**F**) Cell apoptosis analysis. CPP-IL-12 increased and laser treatment further increased the number of apoptotic cells. (**G**) Immunofluorescence. Green color, CALR expression. Scale bars=2 μm. (**H, I**) ELISA analysis of extracellular and intracellular HMGB1 levels, respectively. $^{*}P < 0.05$, $^{**}P < 0.01$, ANOVA. (**J**) ATP levels. The ATP levels decreased in CPP-IL-12-treated cells, and laser treatment further reduced ATP content. $^{**}P < 0.01$, ANOVA. (**K**) CPP increased CD80$^+$/CD86$^+$ expression of DC.

CPP-IL-12 Inhibited the Proliferation of Melanoma Cell Xenografts

The B16-F10 cells expressed in IL-12 or control groups were subcutaneously injected into the backs of C57BL/6 mice to produce xenografts and investigate the role of CPP-IL-12 in regulating melanoma cell proliferation in vivo. After 1 week, the tumors treated with 100 μL of CPP-IL-12 (1mg/mL) or CPP-NC with or without laser treatment (1.5 weeks, 3 min) for 2 days were approximately 1 cm^3 (Figure 3A). After another week, the mice were euthanized, and the tumors were estimated. The results demonstrated that the tumors were considerably smaller and significantly reduced in CPP-IL-12-treated xenografts than in the CPP-control group (Figure 3B and C). In addition, IL-12 remarkably inhibited the volume of xenografts in the CPP-IL-12-treated group compared with that in the control group (Figure 3D). Combined with photosensitive therapy, laser treatment can reduce the growth, weight and volume of tumor xenografts (Figure 3B-D). HE staining demonstrated that the growth of tumor xenografts was suppressed in the CPP-IL-12-treated group and

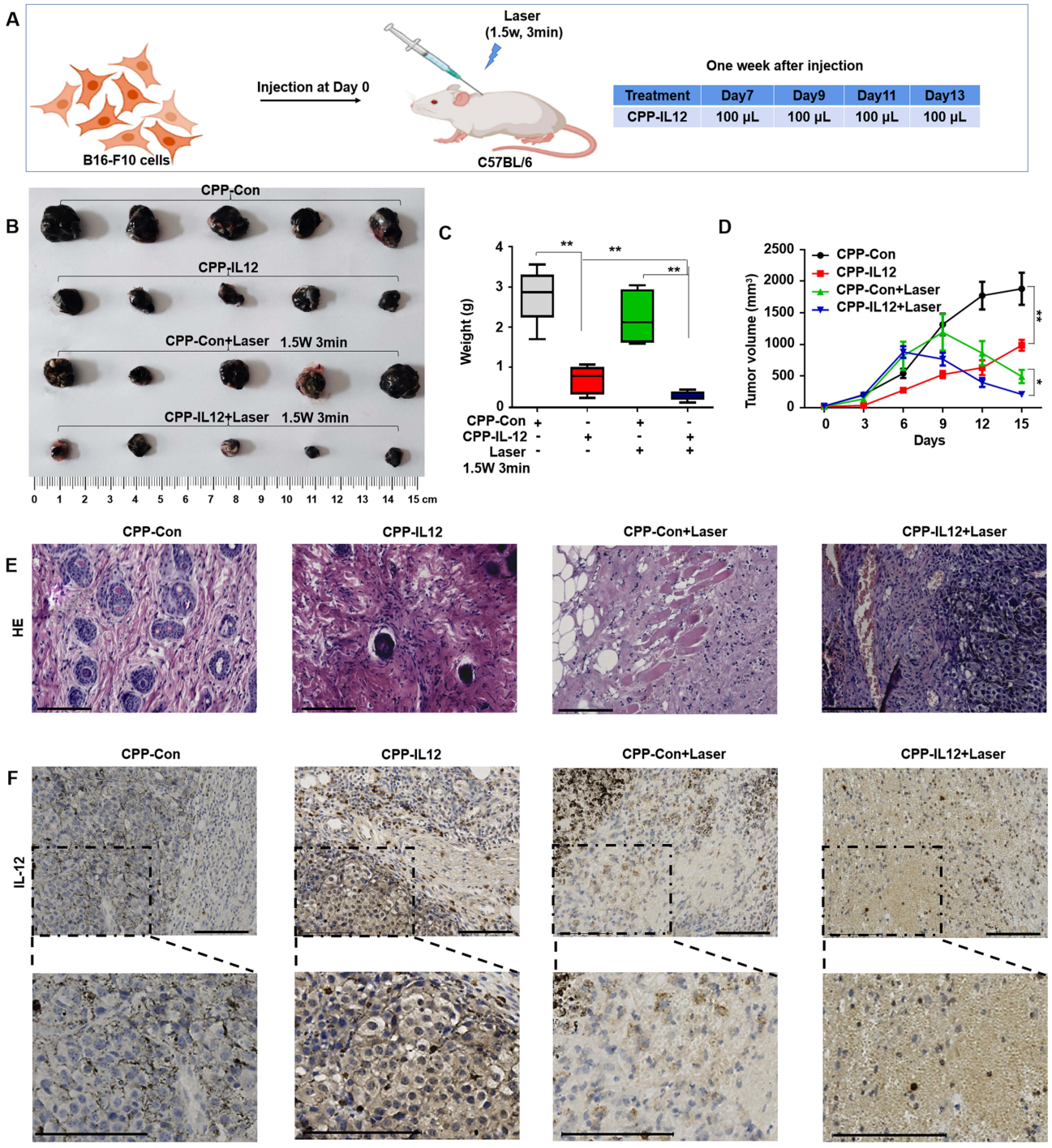

Figure 3 CPP-IL-12 suppressed melanoma cell growth in vivo. (**A**) Schematic illustration of in vivo study. (**B**) The xenografts dissected from mice. (**C, D**) The weights and volumes of xenografts were analyzed. Data were presented as the mean ± SD or median (interquartile range). n=4 or 5, $^{**}P < 0.01$, $^{*}P < 0.05$; Student's *t*-test or Mann–Whitney *U*-test. (**E**) HE staining demonstrated that CPP-IL-12 suppressed and laser further inhibited the growth of tumor xenografts in vivo. (**F**) The levels of IL-12 in tumor xenografts analyzed by immunohistochemistry staining. The brown signal indicated the expression of IL-12 in the tissue, the blue signal was nuclear of cells. There was more IL-12 expression in CPP-IL-12 treated groups. Scale bars=125 μm.

significantly reduced in the CPP-IL-12+laser-treated group compared with those in the control groups (Figure 3E). Immunohistochemical staining was used to analyze the IL-12 levels in tumor xenografts, and the results showed that higher IL-12 expression in the CPP-IL-12-treated or CPP-IL-12+laser-treated xenografts than in the control groups (Figure 3F).

The abovementioned results showed that CPP-IL-12 overexpressed IL-12 and suppressed B16-F10 cell growth in vitro and in vivo, which may be related to ICD releasing DAMPs. The CALR levels in tumor xenograft tissues were analyzed to further investigate whether the role of IL-12 in suppressing cancer cell proliferation in vivo is associated to CALR expression. The results showed that the CALR levels were higher in CPP-IL-12-treated tumor tissues than in the CPP-Con group, and laser treatment further increased CALR expression (Figure 4A), indicating that the suppressive role of IL-12 is related to the regulation of CALR expression.

CPP-IL-12 Promoted Systemic Antitumor Immunity in Xenograft Mice

IL-12 is an activator of DC and NK cells, and it plays an important role in systemic antitumor immunity.[32] After mice were euthanized and the lymph glands were isolated from their groin, armpit, and neck of mice, the cells were separated for detection. The results demonstrated that the $CD80^+/CD86^+$ expression of DC from these lymph glands in CPP-IL-12-treated or CPP-IL-12+laser-treated xenografts increased compared with that in the control groups (Figure 4B). In addition, IL-12 can activate $CD4^+$ T cells[34] and enhance the function of tumor-reactive $CD8^+$ T cells.[35] In CPP-IL-12-treated mice, the number of $CD3^+/CD8^+$T cells from the spleen increased compared with that in the control groups, and laser treatment can further increase the number of $CD3^+/CD8^+$T cells (Figure 4C). Moreover, the number of $CD3^+/CD4^+$ T cells from the spleen of CPP-IL-12-treated mice increased in compared with that of the controls, and laser treatment further increased this number (Figure 4D). These results indicated that CPP-IL-12 treatment may promote antitumor immunity by activating DC, $CD4^+$ T, and $CD8^+$ T cells.

Then, the expression levels of $CD8^+$ and $CD4^+$ in xenograft tumors were analyzed. Immunohistochemical staining showed that the IL-12 and CD8 expression levels were higher in the CPP-IL-12-treated or CPP-IL-12+laser-treated xenografts than that in the control groups (Figure 5A and B). Similar results of $CD4^+$ expression were revealed in CPP-IL-12-treated or CPP-IL-12+laser-treated xenografts (Figure 5C). The results indicated that the anticancer role of CPP-IL-12 may be related to the activation of $CD8^+$ T and $CD4^+$ T cells.

The anticancer activity of antitumor immunity is associated with the releasing levels of IL-12, granzyme B, IFN-γ, and TNF-α. The levels of granzyme B (Figure 5D), IFN-γ (Figure 5E), and TNF-α (Figure 5F) in CPP-IL-12-treated or CPP-IL-12+laser-treated xenografts increased compared with those in the control treatment. Moreover, the serum IL-12 levels in CPP-IL-12-treated or CPP-IL-12+laser-treated mice significantly increased compared with those in the control mice (Figure S2). Similar increased levels of granzyme B (Figure 5G), IFN-γ (Figure 5H), and TNF-α (Figure 5I) were observed in the CPP-IL-12-treated or CPP-IL-12+laser-treated mice, indicating these factors participate in the anticancer role of CPP-IL-12.

CPP-IL-12 Suppression of the Growth of Local and Distant Tumor

Next, the local tumor was treated with CPP-IL-12 and laser, whereas the distant tumor was untreated as controls to further investigate whether CPP-IL-12 treatment could affect the growth of the secondary tumor (Figure 6A). The results showed that the combination treatment of CPP-IL-12 and laser not only inhibited the growth of local xenografts (Figure 6B-D), but clearly suppressed the growth of the distant untreated tumor (Figure 6E-G). In serum, the levels of IFN-γ (Figure 6H), TNF-α (Figure 6I), and granzyme B (Figure 6J) in CPP-IL-12 and CPP-IL-12+laser-treated mice increased compared with those in the control-treated group, indicating the suppressive roles of CPP-IL-12 in the distant tumors is related to the release of IFN-γ, TNF-α and granzyme B.

The $CD80^+/CD86^+$ expression of DC from the lymph nodes and the activation of $CD8^+$ T and $CD4^+$ T cells in the spleen was analyzed to investigate the effect of CPP-IL-12 on the growth of the local or distant tumors. The $CD80^+/CD86^+$ expression of DC in the lymph glands of CPP-IL-12 or CPP-IL-12+laser-treated mice increased compared with that in the control groups (Figure 6K). Similarly, the expression levels of $CD4^+$ and $CD8^+$ were higher in the CPP-IL-12 or CPP-IL-12+laser-treated xenograft mice (Figure 6L and M). Immunohistochemistry staining revealed that the levels of $CD8^+$ and $CD4^+$ in the CPP-IL-12 or CPP-IL-12+laser-treated xenografts were high (Figure 6N and O). These results indicated that the possible mechanism of the anticancer role of CPP-IL-12 may be as follows: the local treatment of CPP-IL-12 activates $CD8^+$ T and $CD4^+$ T cells and as release IFN-γ, TNF-α and granzyme B, which further traffic through the blood circulation to regulate the growth of the distant untreated tumors (Figure 6A).

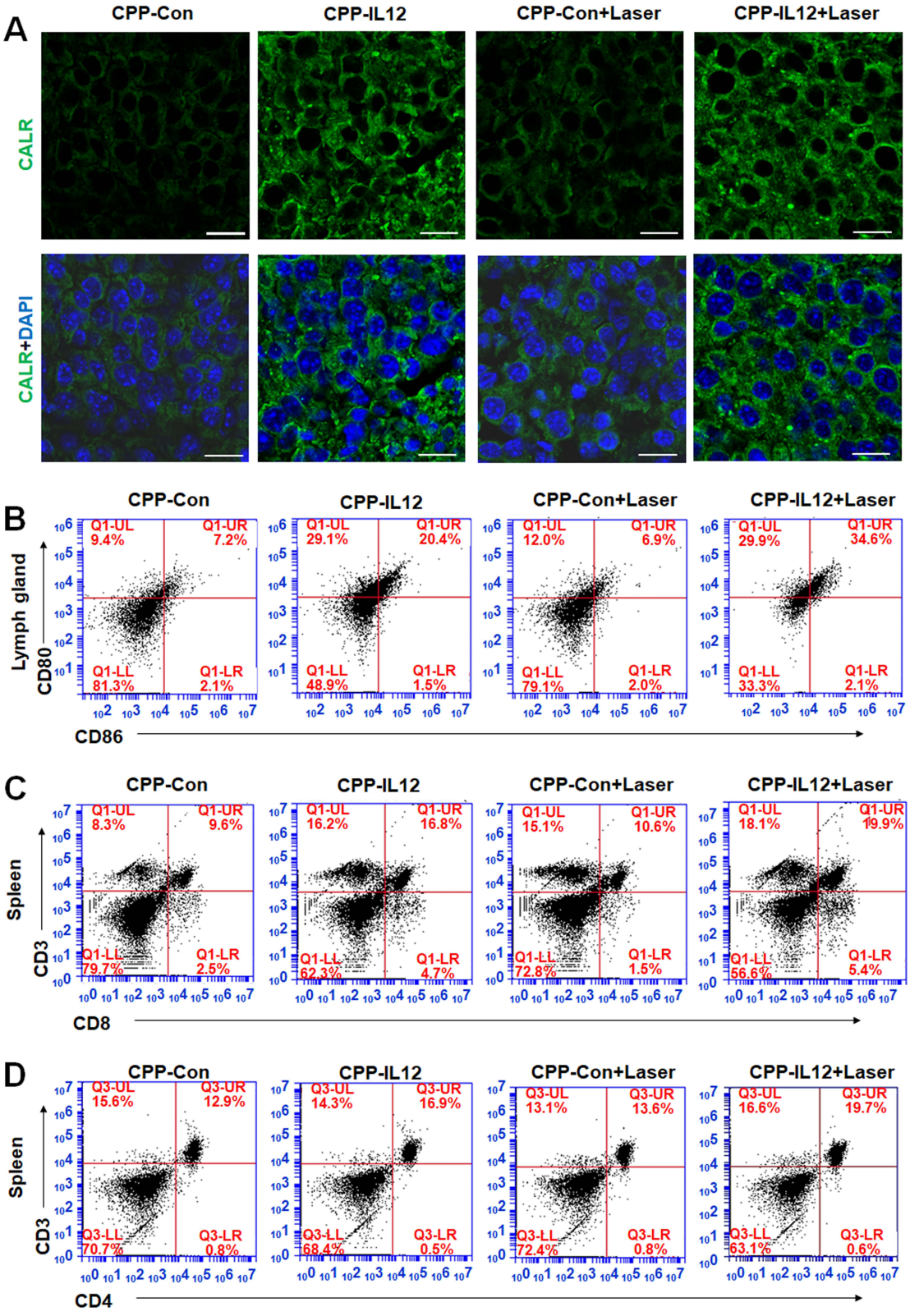

Figure 4 CPP-IL-12 promoted systemic antitumor immunity. (**A**) Analyzing CALR expression in tissues by immunofluorescence. Green color, CALR expression. Scale bars=20 μm. (**B**) CPP-IL-12 increased $CD80^+/CD86^+$ expression of DC in lymph glands. (**C**) CPP-IL-12 increased the number of $CD3^+/CD8^+$T cells from spleen. (**D**) CPP-IL-12 increased the number of $CD3^+/CD4^+$T cells from spleen.

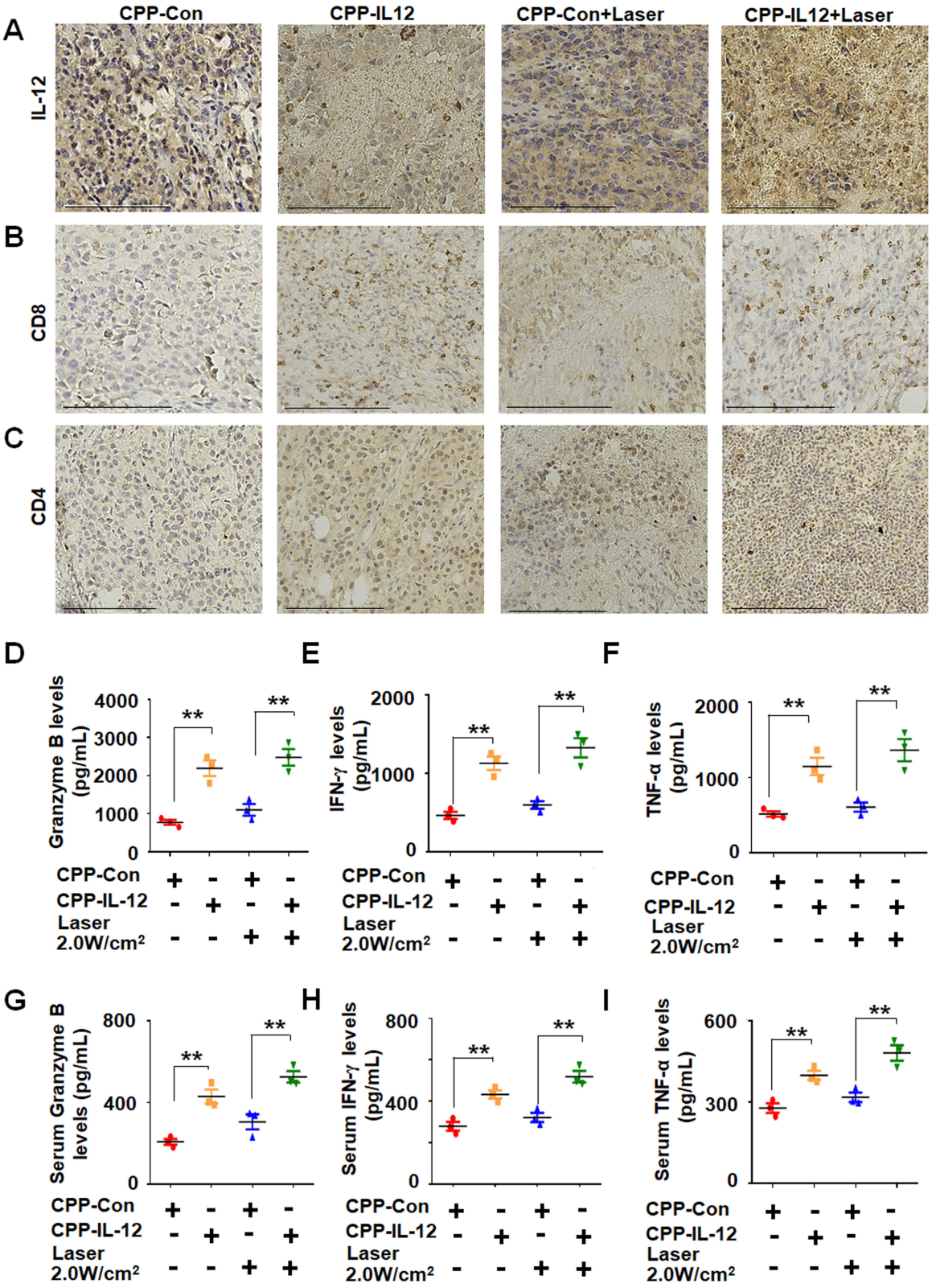

Figure 5 CPP-IL-12 increased the expression of CD4, CD8, granzyme B, IFN-γ and TNF-α. (**A**) CPP-IL-12 increased IL-12 levels in tumor xenografts. Scale bars =125 μm. (**B**) The levels of CD8 were increased in tumor xenografts analyzed by immunohistochemistry staining. Scale bars =125 μm. (**C**) CPP-IL-12 increased CD4 expression in tumor xenografts. Scale bars=125 μm. (**D**) ELISA analysis showed that Granzyme B levels increased in CPP-IL-12-treated tumor xenografts. $^{**}P< 0.01$, ANOVA. (**E**) IFN-γ levels increased in CPP-IL-12-treated tumor xenografts. $^{**}P < 0.01$, ANOVA. (**F**) TNF-α levels increased in CPP-IL-12-treated tumor xenografts. $^{**}P < 0.01$, ANOVA. (**G**) CPP-IL-12 treatment increased granzyme B levels in mouse serum. $^{**}P < 0.01$, ANOVA. (**H**) CPP-IL-12 treatment increased IFN-γ levels in mouse serum. $^{**}P < 0.01$, ANOVA. (**I**) CPP-IL-12 treatment increased TNF-α levels in mouse serum. $^{**}P < 0.01$, ANOVA.

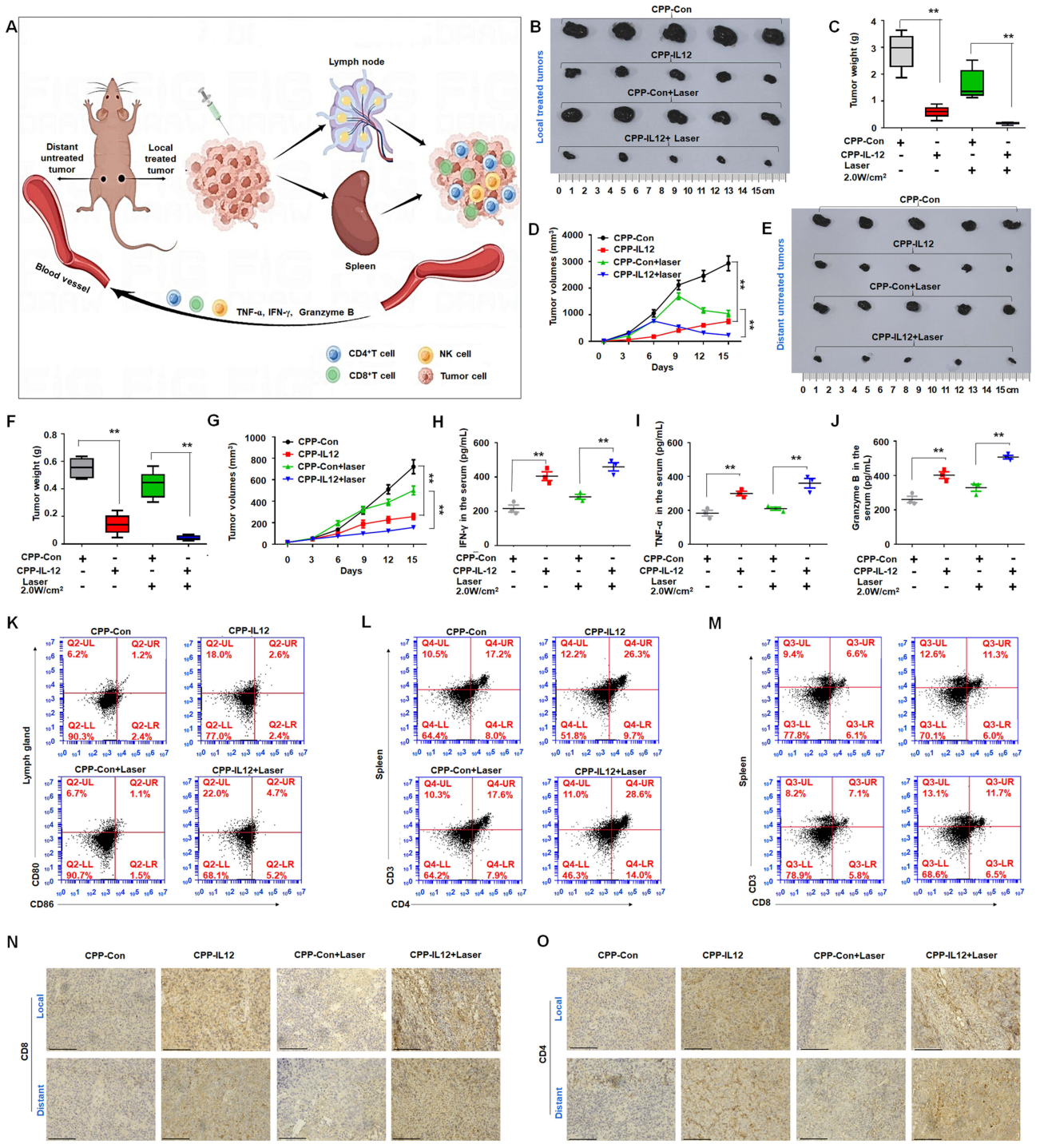

Figure 6 CPP-IL-12 suppressed the growth of local and distant xenografts. (**A**) Schematic description and the mechanism of the effect of local treatment to tumor on distant untreated one. This image was made by using Figdraw software. (**B**–**D**) CPP-IL-12 with laser treatment inhibited the growth, weights and volumes of local xenografts, respectively. $^{**}P < 0.01$, ANOVA. (**E**–**G**) CPP-IL-12 with laser treatment suppressed the growth, weights and volumes of distant tumors, respectively. $^{**}P < 0.01$, ANOVA. (**H**–**J**) ELISA analysis showed that IFN-γ, TNF-α, and granzyme B levels were increased in the serum of CPP-IL-12-treated mice, respectively. $^{**}P < 0.01$, ANOVA. (**K**) $CD80^+/CD86^+$ expression of DC was increased in the lymph glands of CPP-IL-12-treated mice. (**L**) CD4 expression of T cells was increased in the spleens of CPP-IL-12-treated mice. (**M**) CD8 expression was increased in the spleens of CPP-IL-12-treated mice. (**N, O**) The CD8 and CD4 levels were analyzed by immunohistochemistry staining, respectively. Scale bars=125 μm.

Investigation of Toxicity and Distribution of Nanoparticles in vivo

After the C57BL/6 mice were intraperitoneally injected with CPP, the organs were dissected, and pathological tissue sections were analyzed to detect the toxicity of CPP in vivo. HE staining indicated that the injection of CPP did not lead to a significant damage to the organs of the C57BL/6 mice compared with control treatment (Figure 7A). Hemolysis of red blood cells from the C57BL/6 mice was detected to evaluate the blood compatibility of nanoparticles in contact with blood. No significant hemolysis was observed when erythrocytes were treated with 20 μg/mL CPP for 3─24 h. However, significant hemolysis was detected when RBCs were incubated with 40 and 80 μg/mL of CPP for 3 to 24 h, and hemolysis was dependent on concentration over time (Figure 7B and C). The CY5.5-labeled CPP was injected through the tail vein of mice and analyzed using a small animal PET imager system to study the distribution of CPP in mice. The images showed that CY5.5-labeled CPP primarily accumulated in the lung, liver, and kidney of the C57BL/6 mice (Figure 7D).

Discussion

Cancer immunotherapy, which can prolong progression-free survival and overall survival, has incomparable advantages over the traditional anti-tumor therapy.[36] However, it still suffers from drug resistance,[37] low response rates, severe adverse reactions, and high costs; thus, only few patients clinically benefit from immunotherapy.[38] Therefore, in response to complex needs in clinical applications, potential combining strategies should be established to improve the anti-tumor therapeutic effect. In this study, a new antitumor strategy based on CPP-IL-12 nanoparticles was provided. The strategy significantly suppressed melanoma cell proliferation in the local treated tumors and the distant untreated tumors. The mechanism of IL-12 delivery by CPP-IL-12 involves immunotherapy and PTT. On the one hand, combined with PTT, CPP-IL-12 induced IL-12 expression and ICD in tumor environment. On the other hand, ICD further activated DCs, NK cells, and T cells to promote anti-tumor immunity (Figure 7E).

These findings extend those of immunotherapy, and provide a more efficient, without drug resistance immunotherapy for cancer treatment. Tumor immunotherapy exerts its anti-tumor effects by stimulating immune system of the body, or targeting tumor microenvironment. Although various of tumor immunotherapeutic drugs have been found, the delivery of them has become a problem. Inorganic nanoparticles emerged as a possible way for tumor therapy due to their biocompatibility, high drug loading capacity, easy modification and potential photothermal therapy ability.[39,40] Therefore, nanoparticles greatly improved the effect of immunotherapy at all aspects.

Calcium, an essential element for cells, has numerous physiological activities including calcium signaling.[41] In human cells, Ca^{2+} activates calmodulin-dependent protein kinases, which enhance or repress the transcription of specific genes.[42] Ca^{2+} concentration is tightly controlled in cell, and an imbalance can cause severe cellular responses such as induction of cell apoptosis or autophagy.[41] Furthermore, a high concentration of Ca^{2+} in cell may lead to mitochondrion-related oxidative stress, leading to cancerous cellular apoptosis.[42] $CaCO_3$ nanoparticles can release Ca^{2+} in tumor microenvironment because of their pH-dependent properties, which could result in calcium overload for cancer therapy through photothermal and ICD.[23] Therefore, $CaCO_3$ nanoparticles were developed in the present study to investigate their application for cancer therapy. The results showed that CPP treatment increased ROS levels, and laser treatment can further increase these levels, revealing that $CaCO_3$ can be used as drug release systems of antitumor activity by ROS and PTT.

In addition, interleukin-12-expressive plasmid was designed to express IL-12. Compared with those study for mRNA or circRNA delivery,[43,44] plasmid DNA is more stable and not easy to be degraded. Thus, the effect of DNA in tumor immunotherapy may be better than that of RNA to some extent. Most notably, to our knowledge, a new nanoparticle (CPP) was constructed to investigate the effect of IL-12 combining with carbonate calcium nanoparticles in melanoma treatment. IL-12 can enhance the function of tumor-reactive $CD8^+$ T cells, which have been used to stimulate immune cells at the tumor site for tumor therapy.[35] Li et al reported that intratumoral administration of lipid nanoparticles to overexpress IL-12 can stimulate tumor cell ICD,[45] which is accompanied by the release of CALR, ATP, and HMGB1 to activate APCs to kill tumor cells.[32] The IL-12 of nanoparticles can achieve cancer immunotherapy through ICD. The data also showed a significant increase CALR expression, extracellular HMGB1, and ATP levels as ICD biomarkers. ICD-induced therapies are strictly associated with DC engagement.[33] CPP-IL-12 and laser treatment further increased the $CD80^+/CD86^+$ expression of DC compared with control treatment, indicating that CPP-IL-12-induced-ICD is related to the activation of DC. IL-12 is also an activator of DC and NK cells, which is crucial to antitumor immunity.[32] In the

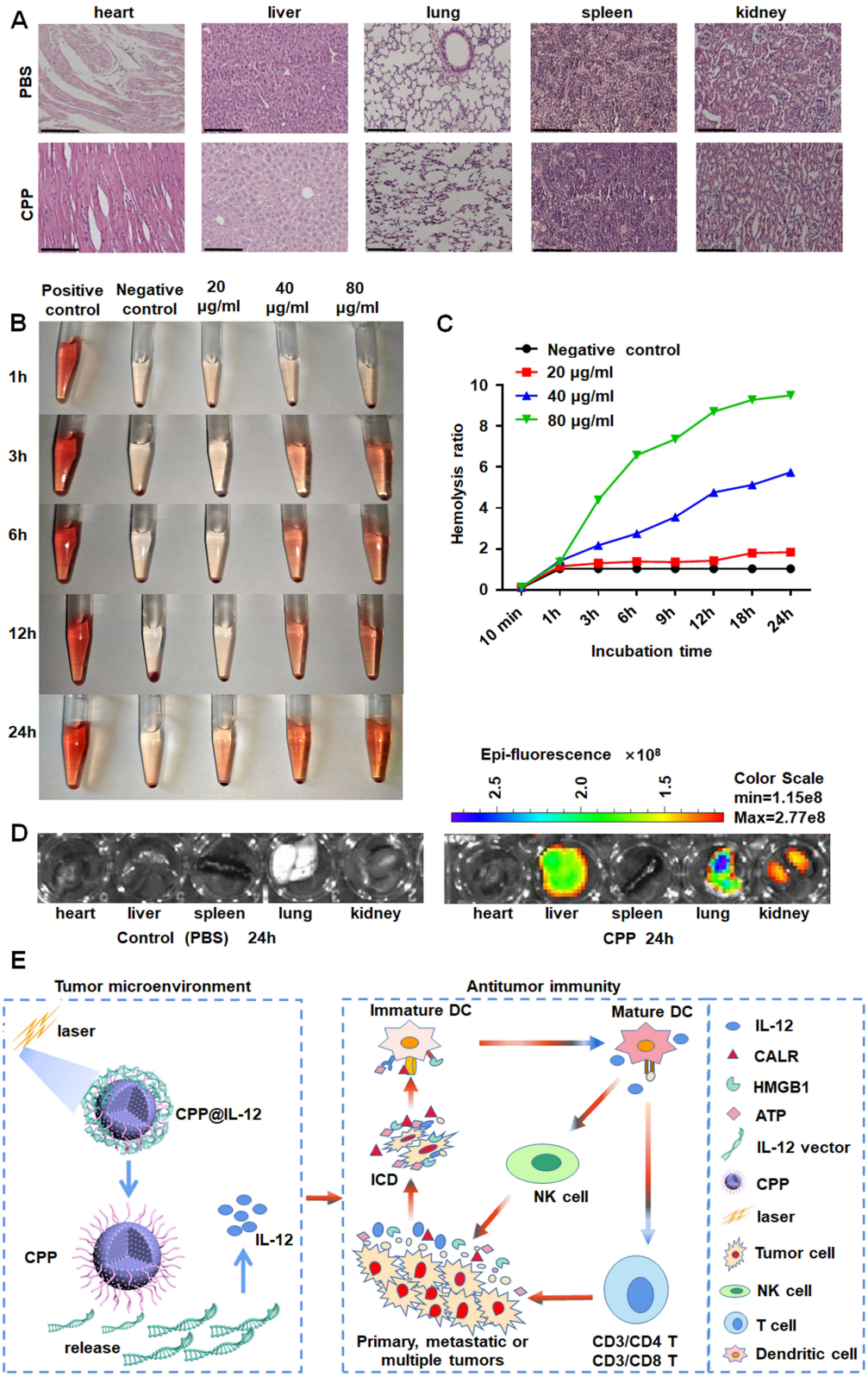

Figure 7 Analyzing the distribution and toxicity of CPP. (**A**) HE staining demonstrated CPP did not lead to significant damage to the organs of mice. Scale bars=125 μm. (**B, C**) The blood compatibility of nanoparticles was evaluated by Hemolysis test. (**D**) The distribution of CPP in mice. (**E**) CPP-IL-12 nanoparticles could significantly suppress melanoma cell proliferation. On one hand, IL-12 delivery by CPP-IL-12 involves immunotherapy and PTT, which induced IL-12 expression and ICD in tumor environment. On the other hand, the ICD would further activate dendritic cells, NK cells, and T cells to promote antitumor immunity.

https://doi.org/10.2147/IJN.S442446 DovePress

present study, the $CD80^+/CD86^+$ expression of DC from the lymph glands in CPP-IL-12-treated or CPP-IL-12+laser-treated xenografts increased. Moreover, in CPP-IL-12-treated mice, the number of $CD3^+/CD4^+$ T and $CD3^+/CD8^+$ T cells from the spleen increased compared with that in the control groups, and laser treatment can further increase the numbers. Furthermore, the granzyme B, IFN-γ, and TNF-α levels in the serum of CPP-IL-12-treated mice can be increased. These results revealed that IL-12 can activate $CD4^+$ T cells[34] and enhance the role of tumor-reactive $CD8^+$ T cells.[35] Our results provide compelling evidence for mice melanoma immunotherapy and suggest that it may be a better approach to induce immune response of the body itself.

However, some limitations are worth noting. Although our results displayed good treatment effect of melanoma xenografts in situ, whether the new nanoparticle can suppress the metastasis of melanoma or other tumors is still unclear. Melanoma, the most aggressive form of malignancy arising from melanocytes, is frequently characterized metastasis.[46] Future work should therefore include work designed to evaluate whether the tumor metastasis could be well suppressed by the new nanoparticles. Moreover, although no evident cytotoxicity to NIH3T3 cells was found when the nanomaterial dose increased from 10 to 30 μg/mL of CPP, the cytotoxicity of higher concentrations still needs to be investigated in the future.

Conclusion

The novel CPP-IL-12 could overexpress IL-12 in melanoma cells and achieve immunotherapy to melanoma through inducing ICD, activating $CD4^+$ T cell, and enhancing the function of tumor-reactive $CD8^+$ T cells. This study not only provides a new approach for immunotherapy to melanoma, but also indicates a potential application of CPP-IL-12 in treating of primary and abscopal or multiple tumors.

Acknowledgments

We thank professional editing support from ShineWrite.com (service@shinewrite.com) for editing the English text of a draft of this manuscript. We created schematic illustration of in vivo study using the Figdraw software.

Funding

The present study was supported by the National Natural Science Foundation of China (No.81772281, 31371321), the Shandong Science and Technology Committee (No. ZR2022LSW002, ZR2020KH015), the Education Department of Shandong Province (2019KJK014, 2021KJ101), and the Science Fund of Shandong Laboratory of Advanced Materials and Green Manufacturing (Yantai) (AMGM2023F16).

Disclosure

The authors declare no conflicts of interest in this work.

References

1. Anselmo AC, Mitragotri S. A Review of Clinical Translation of Inorganic Nanoparticles. *AAPS J*. 2015;17(5):1041–1054. doi:10.1208/s12248-015-9780-2
2. Park DJ, Min KH, Lee HJ, et al. Photosensitizer-loaded bubble-generating mineralized nanoparticles for ultrasound imaging and photodynamic therapy. *J Mater Chem B*. 2016;4(7):1219–1227. doi:10.1039/c5tb02338f
3. Zhu Y, Yang Z, Dong Z, et al. CaCO(3)-Assisted Preparation of pH-Responsive Immune-Modulating Nanoparticles for Augmented Chemo-Immunotherapy. *Nanomicro Lett*. 2020;13(1):29. doi:10.1007/s40820-020-00549-4
4. Roth R, Schoelkopf J, Huwyler J, Puchkov M. Functionalized calcium carbonate microparticles for the delivery of proteins. *Eur J Pharm Biopharm*. 2018;122:96–103. doi:10.1016/j.ejpb.2017.10.012
5. Li H, Zhang X, Lin X, et al. CaCO3 nanoparticles pH-sensitively induce blood coagulation as a potential strategy for starving tumor therapy. *J Mat Chem B*. 2020;8(6):1223–1234. doi:10.1039/c9tb02684c
6. Guan X, Guo Z, Wang T. A pH-Responsive Detachable PEG Shielding Strategy for Gene Delivery System in Cancer Therapy. *Biomacromolecules*. 2017;18(4):1342–1349. doi:10.1021/acs.biomac.7b00080
7. Lv P, Zhou C, Zhao Y, Liao X, Yang B. Modified-epsilon-polylysine-grafted-PEI-β-cyclodextrin supramolecular carrier for gene delivery. *Carbohydr. Polym.* 2017;168:103–111. doi:10.1016/j.carbpol.2017.02.036
8. Liu Y, Bhattarai P, Dai Z, Chen X. Photothermal therapy and photoacoustic imaging via nanotheranostics in fighting cancer. *Chem Soc Rev*. 2019;48(7):2053–2108. doi:10.1039/c8cs00618k
9. Ye L, Chen Y, Mao J, Lei X, Yang Q, Cui C. Dendrimer-modified gold nanorods as a platform for combinational gene therapy and photothermal therapy of tumors. *J Exp Clin Cancer Res*. 2021;40(1):303. doi:10.1186/s13046-021-02105-3

10. Cai Z, Xin F, Wei Z, et al. Photodynamic Therapy Combined with Antihypoxic Signaling and CpG Adjuvant as an In Situ Tumor Vaccine Based on Metal-Organic Framework Nanoparticles to Boost Cancer Immunotherapy. *Adv Healthc Mater*. 2020;9(1):e1900996. doi:10.1002/adhm.201900996
11. Ye X, Liang X, Chen Q, et al. Surgical Tumor-Derived Personalized Photothermal Vaccine Formulation for Cancer Immunotherapy. *ACS Nano*. 2019;13(3):2956–2968. doi:10.1021/acsnano.8b07371
12. Liu Y, Ai K, Liu J, Deng M, He Y, Lu L. Dopamine-Melanin Colloidal Nanospheres: an Efficient Near-Infrared Photothermal Therapeutic Agent for In Vivo Cancer Therapy. *Adv. Mater.* 2012;25(9):1353–1359. doi:10.1002/adma.201204683
13. Chen Y, Ai K, Liu J, Ren X, Jiang C, Lu L. Polydopamine-based coordination nanocomplex for T1/T2 dual mode magnetic resonance imaging-guided chemo-photothermal synergistic therapy. *Biomaterials*. 2016;77:198–206. doi:10.1016/j.biomaterials.2015.11.010
14. Ge R, Li X, Lin M, et al. Correction to Fe3O4@polydopamine Composite Theranostic Superparticles Employing Preassembled Fe3O4 Nanoparticles as the Core. *ACS Appl. Mater. Interfaces*. 2021;13(15):18389–18390. doi:10.1021/acsami.1c04988
15. Wang H, Mooney DJ. Biomaterial-assisted targeted modulation of immune cells in cancer treatment. *Nat Mater*. 2018;17(9):761–772. doi:10.1038/s41563-018-0147-9
16. Qiu N, Wang G, Wang J, et al. Tumor-Associated Macrophage and Tumor-Cell Dually Transfecting Polyplexes for Efficient Interleukin-12 Cancer Gene Therapy. *Adv Mater*. 2021;33(2):e2006189. doi:10.1002/adma.202006189
17. Tugues S, Burkhard SH, Ohs I, et al. New insights into IL-12-mediated tumor suppression. *Cell Death Differ*. 2015;22(2):237–246. doi:10.1038/cdd.2014.134
18. Etxeberria I, Bolanos E, Quetglas JI, et al. Intratumor Adoptive Transfer of IL-12 mRNA Transiently Engineered Antitumor CD8(+) T Cells. *Cancer Cell*. 2019;36(6):613–629 e7. doi:10.1016/j.ccell.2019.10.006
19. Agliardi G, Liuzzi AR, Hotblack A, et al. Intratumoral IL-12 delivery empowers CAR-T cell immunotherapy in a pre-clinical model of glioblastoma. *Nat Commun*. 2021;12(1):444. doi:10.1038/s41467-020-20599-x
20. Algazi AP, Twitty CG, Tsai KK, et al. Phase II Trial of IL-12 Plasmid Transfection and PD-1 Blockade in Immunologically Quiescent Melanoma. *Clin Cancer Res*. 2020;26(12):2827–2837. doi:10.1158/1078-0432.CCR-19-2217
21. Yu L, Hu P, Chen Y. Gas-Generating Nanoplatforms: material Chemistry, Multifunctionality, and Gas Therapy. *Adv Mater*. 2018;30(49):e1801964. doi:10.1002/adma.201801964
22. Li B, Gong T, Xu N, et al. Improved Stability and Photothermal Performance of Polydopamine-Modified Fe(3) O(4) Nanocomposites for Highly Efficient Magnetic Resonance Imaging-Guided Photothermal Therapy. *Small*. 2020;16(45):e2003969. doi:10.1002/smll.202003969
23. Zheng P, Ding B, Jiang Z, et al. Ultrasound-Augmented Mitochondrial Calcium Ion Overload by Calcium Nanomodulator to Induce Immunogenic Cell Death. *Nano Lett*. 2021;21(5):2088–2093. doi:10.1021/acs.nanolett.0c04778
24. Zhang Q, Yan YF, Lv Q, et al. miR-4293 upregulates lncRNA WFDC21P by suppressing mRNA-decapping enzyme 2 to promote lung carcinoma proliferation. *Cell Death Dis*. 2021;12(8):735. doi:10.1038/s41419-021-04021-y
25. Hao R, Hu J, Liu Y, et al. RFWD2 Knockdown as a Blocker to Reverse the Oncogenic Role of TRIB2 in Lung Adenocarcinoma. *Front Oncol*. 2021;11:733175. doi:10.3389/fonc.2021.733175
26. Maleki Dizaj S, Sharifi S, Ahmadian E, Eftekhari A, Adibkia K, Lotfipour F. An update on calcium carbonate nanoparticles as cancer drug/gene delivery system. *Expert Opin Drug Deliv*. 2019;16(4):331–345. doi:10.1080/17425247.2019.1587408
27. Wang W, Tang Z, Zhang Y, Wang Q, Liang Z, Zeng X. Mussel-Inspired Polydopamine: the Bridge for Targeting Drug Delivery System and Synergistic Cancer Treatment. *Macromol Biosci*. 2020;20(10):e2000222. doi:10.1002/mabi.202000222
28. Glass SB, Gonzalez-Fajardo L, Beringhs AO, Lu X. Redox Potential and ROS-Mediated Nanomedicines for Improving Cancer Therapy. *Antioxid Redox Signal*. 2019;30(5):747–761. doi:10.1089/ars.2017.7370
29. Kuan CY, Lin YY, Yang IH, et al. The Synthesis of Europium-Doped Calcium Carbonate by an Eco-Method as Free Radical Generator Under Low-Intensity Ultrasonic Irradiation for Body Sculpture. *Front Bioeng Biotechnol*. 2021;9:765630. doi:10.3389/fbioe.2021.765630
30. Zaharoff DA, Hance KW, Rogers CJ, Schlom J, Greiner JW. Intratumoral immunotherapy of established solid tumors with chitosan/IL-12. *J Immunother*. 2010;33(7):697–705. doi:10.1097/CJI.0b013e3181eb826d
31. Duan X, Chan C, Lin W. Nanoparticle-Mediated Immunogenic Cell Death Enables and Potentiates Cancer Immunotherapy. *Angew Chem Int Ed Engl*. 2019;58(3):670–680. doi:10.1002/anie.201804882
32. Fucikova J, Kepp O, Kasikova L, et al. Detection of immunogenic cell death and its relevance for cancer therapy. *Cell Death Dis*. 2020;11(11):1013. doi:10.1038/s41419-020-03221-2
33. Lamberti MJ, Nigro A, Mentucci FM, Rumie Vittar NB, Casolaro V, Dal Col J. Dendritic Cells and Immunogenic Cancer Cell Death: a Combination for Improving Antitumor Immunity. *Pharmaceutics*. 2020;12(3):56.
34. Xiao Z, Kandel A, Li L. Synergistic Activation of Bovine CD4+ T Cells by Neutrophils and IL-12. *Pathogens*. 2021;10(6).
35. Salem ML, Salman S, Barnawi IO. Brief in vitro IL-12 conditioning of CD8 (+)T Cells for anticancer adoptive T cell therapy. *Cancer Immunol Immunother*. 2021;70(10):2751–2759. doi:10.1007/s00262-021-02887-7
36. Tan S, Li D, Zhu X. Cancer immunotherapy: pros, cons and beyond. *Biomed Pharmacother*. 2020;124:109821. doi:10.1016/j.biopha.2020.109821
37. Guo X, Gao C, Yang D-H, Li S. Exosomal circular RNAs: a chief culprit in cancer chemotherapy resistance. *Drug Resist Updates*. 2023;67. doi:10.1016/j.drup.2023.100937
38. Han S, Shuen WH, Wang WW, Nazim E, Toh HC. Tailoring precision immunotherapy: coming to a clinic soon? *ESMO Open*. 2020;5 Suppl 1 (Suppl 1):e000631. doi:10.1136/esmoopen-2019-000631
39. Zhu X, Li S. Nanomaterials in tumor immunotherapy: new strategies and challenges. *Mol Cancer*. 2023;22(1):1342–1349. doi:10.1186/s12943-023-01797-9
40. Chen Z, Yue Z, Yang K, et al. Four Ounces Can Move a Thousand Pounds: the Enormous Value of Nanomaterials in Tumor Immunotherapy. *Adv. Healthcare Mater.* 2023;12(26).
41. Maklad A, Sharma A, Azimi I. Calcium Signaling in Brain Cancers: roles and Therapeutic Targeting. *Cancers*. 2019;11(2):564.
42. Takemoto-Kimura S, Suzuki K, Horigane SI, et al. Calmodulin kinases: essential regulators in health and disease. *J Neurochem*. 2017;141(6):808–818. doi:10.1111/jnc.14020
43. Cheng Q, Wei T, Farbiak L, Johnson LT, Dilliard SA, Siegwart DJ. Selective organ targeting (SORT) nanoparticles for tissue-specific mRNA delivery and CRISPR–Cas gene editing. *Nature Nanotechnol*. 2020;15(4):313–320. doi:10.1038/s41565-020-0669-6

44. Alkhathami AG, Sahib AS, Al Fayi MS, et al. Glycolysis in human cancers: emphasis circRNA/glycolysis axis and nanoparticles in glycolysis regulation in cancer therapy. *Environ. Res.* 2023:234. doi:10.1016/j.envres.2023.116007
45. Li Y, Su Z, Zhao W, et al. Multifunctional oncolytic nanoparticles deliver self-replicating IL-12 RNA to eliminate established tumors and prime systemic immunity. *Nat Cancer*. 2020;1(9):882–893. doi:10.1038/s43018-020-0095-6
46. Xu M, Li S. Nano-drug delivery system targeting tumor microenvironment: a prospective strategy for melanoma treatment. *Cancer Lett*. 2023;574. doi:10.1016/j.canlet.2023.216397